Tunable, Ultrafast Fiber-Laser Between 1.15 and 1.35 μm for Harmonic Generation Microscopy in Human Skin

Hsiang-Yu Chung, Wei Liu, Qian Cao, Rüdiger Greinert, Franz X. Kärtner, *Fellow, IEEE*, and Guoqing Chang

***Abstract*—We demonstrate a fiber-optic ultrafast tunable source for harmonic generation microscopy (HGM) in human skin. The source is based on a 31-MHz Er-fiber laser followed by self-phase modulation enabled spectral selection (SESS). The resulting pulses are tunable between 1.15 and 1.35 μm with up to >10-nJ pulse energy and ~100-fs pulse duration. We employ this source to drive a scanning microscope for HGM imaging of *ex vivo* human skin. A systematic investigation on imaging depth versus excitation wavelength reveals that excitation wavelengths in the 1.15–1.25 μm range exhibit low optical attenuation within the tissue and allows larger imaging depth for HGM in human skin. HGM driven by fiber-based SESS sources constitutes an enabling tool for noninvasive virtual skin biopsy in clinical applications.**

***Index Terms*—Biomedical imaging, fiber lasers, nonlinear fiber optics, nonlinear optical microscopy, optical harmonic generation.**

I. Introduction

HARMONIC generation microscopy (HGM) is one of the most important modalities for optical virtual skin biopsy [1]–[7]. HGM requires a driving laser system that emits femtosecond pulses, which interact with the skin sample in a nonlinear way to provide imaging contrast. With sub-micron optical resolution, HGM also features low photodamage and low photobleaching because the imaging contrast originates from the intrinsic structure of the sample rather than from the molecular resonance. For example, collagen and elastic fibers in human skin have non-centrosymmetric structure that enables second-harmonic generation (SHG) [1]–[7]. In contrast, third-harmonic generation (THG) arises from the interface and inhomogeneity between nucleus and cytoplasmic membrane, which can provide subcellular information [2]–[4], [6], [7]. Different layers and tissues, e.g., stratum corneum (SC), stratum granulosum (SG), stratum spinosum (SS), and stratum basale (SB) in epidermis can be differentiated from their THG contrast [4], [6], [7].

To date, ultrafast Ti:sapphire lasers are the most popular driving source in implementing HGM. These lasers normally operate at tens-of-MHz repetition rate and produce ~100-fs pulses with their center wavelength tunable in 700–1000 nm. However, the corresponding THG (233–333 nm) falls within ultraviolet (UV) region and suffers from strong water/protein absorption, low objective transmittance, and low sensitivity of the photomultiplier tube (PMT). These disadvantages have stimulated research efforts in developing femtosecond driving sources at longer wavelengths. For example, HGM benefits from a femtosecond driving source in the 1.15–1.35 μm range, because most of the resulting SHG and THG falls in the visible wavelength range and can be efficiently detected by gallium arsenide phosphide PMTs. Longer excitation wavelengths correspond to less photon energy and reduce the risk of photodamage, which also raises the excitation power tolerance. Under 1230-nm excitation, the applied power can be as high as 140 mW [8], while only 6-mW average power can prevent cells from forming clones under 800-nm excitation [9]. Furthermore, the wavelength range 1.15–1.35 μm coincides with one of the bio-tissue transmission windows featuring relatively low optical attenuation caused by scattering and absorption within the tissue [10]–[15]; therefore, an increased imaging depth can be achieved. A detailed comparison has shown that SHG imaging driven by 1250-nm femtosecond pulses can achieve sharp images at a depth of 250 μm in porcine skin, which is twice the imaging depth achieved with 800-nm femtosecond pulses from Ti:sapphire lasers [5].

Several ultrafast laser sources have been implemented to produce femtosecond pulses in the 1.15–1.35 μm wavelength range. Passively mode-locked Cr:forsterite lasers directly emit femtosecond pulses in the wavelength range of 1230–1250 nm [2]–[8], [16]–[18]. Broadly tunable femtosecond pulses can be

Manuscript received March 18, 2018; revised May 30, 2018; accepted July 31, 2018. Date of publication August 9, 2018; date of current version August 24, 2018. This work was supported in part by the Helmholtz Association through the Helmholtz Young Investigator Group under Grant VH-NG-804, in part by the Helmholtz-CAS Joint Research Group under Grant HCJRG 201, and in part by the excellence cluster "The Hamburg Centre for Ultrafast Imaging—Structure, Dynamics and Control of Matter at the Atomic Scale" of the Deutsche Forschungsgemeinschaft under Grant EXC 1074. *(Corresponding authors: Hsiang-Yu Chung; Guoqing Chang.)*

H.-Y. Chung, Q. Cao, and F. X. Kärtner are with the Center for Free-Electron Laser Science, DESY, Hamburg 22607, Germany, and also with the Physics Department, Universität Hamburg, Hamburg 22761, Germany (e-mail: hsiang-yu.chung@cfel.de; qian.cao@desy.de; franz.kaertner@desy.de).

W. Liu was with the Center for Free-Electron Laser Science, DESY, Hamburg 22607, Germany, and also with the Physics Department, Universität Hamburg, Hamburg 22761, Germany. He is now with the SLAC National Laboratory and Stanford University, Menlo Park, CA 94025 USA (e-mail: weiopt@slac.stanford.edu).

R. Greinert is with the Skin Cancer Center Buxtehude, Buxtehude 21614, Germany (e-mail: grein25@gmx.de).

G. Q. Chang was with the Center for Free-Electron Laser Science, DESY, Hamburg 22607, Germany. He is now with the Institute of Physics, Chinese Academy of Sciences, Beijing 100190, China (e-mail: guoqing.chang@iphy.ac.cn).

Color versions of one or more of the figures in this paper are available online at http://ieeexplore.ieee.org.

Digital Object Identifier 10.1109/JSTQE.2018.2864193

obtained from solid-state synchronously pumped optical parametric oscillators [19]–[22] or optical parametric amplifiers [15], [23], [24].

Despite their success, however, these solid-state lasers demand precise cavity-alignment and environmental control (i.e., water cooling, temperature and humidity feedback loop, vibration isolation etc.), which limits the use of HGM to specialized laboratories. In contrast, fiber-optic femtosecond sources based on ultrafast fiber lasers followed by nonlinear wavelength conversion in optical fibers offer a simple and robust solution. Indeed, HGM has been practiced in the 1.15–1.35 μm wavelength range by several groups utilizing fiber-laser based wavelength conversion sources. Normally these HGM driving sources are derived from Er-fiber lasers emitting 1.55-μm pulses, which can be converted to 1.2-μm pulses via fiber-optic Cherenkov radiation [25], [26]. The center wavelength of the resulting pulses is largely fixed by the phase-matching condition required by fiber-optic Cherenkov radiation. Due to the use of highly nonlinear fiber, the 1.2-μm femtosecond source delivers only 1.07-nJ pulse energy [25]. Another fiber-optic nonlinear wavelength conversion mechanism is soliton self-frequency shift (SSFS), which can redshift the output pulse from an Yb-fiber laser to the wavelength range of 1.15–1.35 μm [27]–[29]. It is noteworthy that the resulting Raman soliton energy is limited by the soliton-area-theorem. To increase the soliton pulse energy, higher-order-mode fibers are employed to excite SSFS [30], [31]. Another approach is to employ SSFS in large-mode-area (LMA) rod-type fibers pumped by an Er-fiber laser, which generates Raman soliton pulses at 2.3 μm followed by frequency doubling to 1.15 μm [32]. However, strong absorption in fused silica beyond 2.3 μm prevents achieving femtosecond pulses with wavelength longer than 1.15 μm.

Recently we extended the fiber-optic approach underlying Mamyshev regenerator [33] to produce wavelength widely tunable ($\sim$400 nm) femtosecond pulses [34]–[37]. In this approach, a narrowband input optical spectrum is dramatically broadened inside a short ($<$10-cm length) optical fiber by self-phase modulation (SPM) dominated nonlinearity. Consequently, isolated spectral lobes are developed with a considerable portion of power contained by the leftmost and the rightmost spectral lobes. We then use optical filters to select the leftmost/rightmost spectral lobes, which produces nearly transform-limited $\sim$100-fs pulses with the center wavelength widely tunable. Such SPM-enabled spectral selection (SESS) allows us to derive up to $>$10-nJ, $\sim$100-fs pulses tunable in 1030–1215 nm from an LMA fiber pumped by an Yb-fiber laser at 1030 nm [35]. We also applied SESS to ultrafast Er-fiber lasers and obtained femtosecond pulses tunable from 1.3 μm to 1.7 μm with 15.8-nJ pulse energy at 1.3 μm [37].

In this paper, we improve our Er-fiber laser based SESS source to obtain femtosecond pulses tunable between 1.15 μm and 1.35 μm with pulse energy of 7.2-11.7 nJ. This source is then integrated with a scanning microscope for HGM imaging of *ex vivo* human skin tissue with a focus on investigating imaging performance versus excitation wavelength. We apply five different excitation wavelengths—1.15 μm, 1.2 μm, 1.25 μm, 1.3 μm, and 1.35 μm—with the same peak power after the objective and compare the resulting SHG and THG signal in skin tissue within 300-μm penetration depth. Considering both the sensitivity and gain of the detector, our experimental results show that besides 1.25-μm (Cr:forsterite laser wavelength) excitation, wavelengths at 1.15 μm and 1.2 μm are also suitable for conducting HGM in human skin.

II. Experimental Setup

The experimental setup depicted in Fig. 1 mainly consists of two parts: an Er-fiber laser based SESS source and a scanning harmonic generation microscope.

A. Fiber-Based SESS Source

The driving SESS source is derived from a home-built 31-MHz Er-fiber laser system producing up to 160-nJ, 290-fs pulses after the grating compressor. More details about the laser system can be found in [36]. To implement SESS, we couple the pulses into 8.5-cm dispersion-shifted fiber (DSF) for SPM-dominated spectral broadening. The DSF has a 10-μm mode-field diameter and -10 fs^2/ mm group-velocity dispersion at 1.55 μm. We use a half-wave plate (HWP) and a polarization beam splitter (PBS) to vary the pulse energy coupled into the DSF. The fiber coupling module includes a fiber holder (HFV002, Thorlabs), a 3-axis stage (MAX313D/M, Thorlabs), and an aspheric lens (C240TME-C, Thorlabs) with 8-mm effective focal length. The coupling efficiency under low power is 70%. As the coupled energy is increased from 75 nJ to 100 nJ, the peak wavelength of the leftmost spectral lobe in the broadened spectrum shifts from 1.35 μm to 1.15 μm. Then we use optical bandpass filters (BPFs) to select these spectral lobes for HGM.

Figure 2 (left column) shows the spectra filtered by different BPFs with 50-nm bandwidth centered at 1.15 μm, 1.2 μm, 1.25 μm, 1.3 μm, and 1.35 μm (Edmund Optics). The resulting SESS tunable femtosecond source has an average power of 224–362 mW, corresponding to pulse energy of 7.2-11.7 nJ before the scanning microscope, which meets the requirement ($>$5 nJ) to achieve fine THG contrast [4], [6], [7], [32]. After reaching the thermal equilibrium, the power fluctuation of the filtered spectral lobe from the tunable source between 1.15 μm and 1.35 μm is a couple of percent. Due to the microscope transmittance loss, the maximum available average power after the objective is 83–210 mW (shown in parentheses in the left column of Fig. 2), corresponding to pulse energy of 2.7-6.8 nJ. The red curves in the right column of Fig. 2 show the autocorrelation traces measured after the objective. The full-width at half-maximum (FWHM) duration of these traces is 142–168 fs, from which we estimate the pulse duration to be 92–109 fs, assuming hyperbolic-secant pulse profile with a deconvolution factor of 1.54. The pulses are slightly chirped compared with the calculated transform-limited pulses allowed by the filtered spectra (black dashed curves in the right column of Fig. 2). The characterized average power and pulse duration measured at different wavelength after the objective is later used to calibrate the pulse peak power after the objective. It is noteworthy that we use the term "after the objective" instead of "at the sample surface." The objective is water immersive; however, the characterizations are carried out without water immersion.

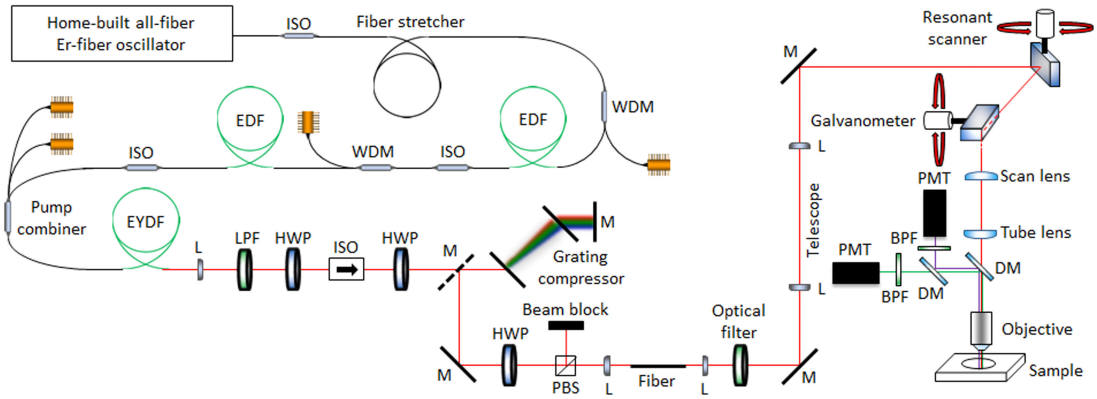

Fig. 1. Schematic setup of the fiber-based SESS source for HGM. ISO: isolator, WDM: wavelength-division multiplexing, EDF: erbium-doped fiber, EYDF: erbium ytterbium co-doped fiber, L: lens, LPF: long pass filter, HWP: half-wave plate, M: mirror, PBS: polarization beam splitter, DM: dichroic mirror, BPF: bandpass filter, PMT: photomultiplier tube.

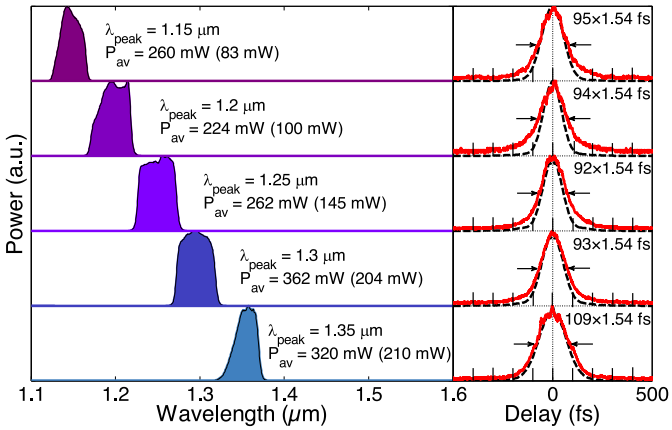

Fig. 2. (Left column) Filtered optical spectra; their peak wavelength and average power are labeled in the figure. Measured power after the objective is shown in the parentheses. (Right column) Measured autocorrelation traces after the objective (red solid curves) and autocorrelation traces calculated from the transform-limited pulses allowed by the filtered spectra (black dashed curves).

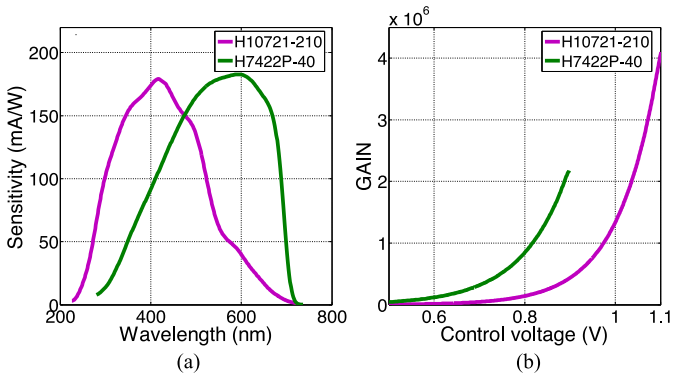

Fig. 3. (a) Cathode radiant sensitivity and (b) gain of the PMTs used for signal detection. H10721-210 (magenta curves) is for THG, and H7422P-40 is for SHG (green curves).

B. Scanning Microscope

We use a telescope before the excitation beam entering the scanning microscope (MPM-2PKIT, Thorlabs) to match the beam size to the objective (XLPLN25XWMP2, Olympus) clear aperture. The scanning system consists of a resonant scanner (8 kHz) and a mirror galvanometer (up to 30 Hz). The 25× water immersive objective has 1.05 numerical aperture (NA) and 2-mm working distance. The emitted signal is epi-collected by the same objective and reflected by a DM (Di02-R1064-25 × 36, Semrock). Another DM with different edge wavelength (FF562-Di03-25 × 36 or Di02-R405-25 × 36, Semrock) further separates SHG and THG from different excitation. A motorized stage provides vertical movement with adjustable velocity to observe the sample at the different depth from the surface, which ensures that imaging can be continuously recorded.

Figure 3(a) depicts the cathode radiant sensitivity of the PMTs for signal detection, with the voltage dependent gain shown in Fig. 3(b) [38]. For the excitation wavelength in 1.15–1.35 μm, we use PMT (H7422P-40, Hamamatsu) with the peak sensitivity at 580 nm [green curve in Fig. 3(a)] to detect the corresponding SHG (575-675 nm). The THG (383–450 nm) is detected by another PMT (H10721-210, Hamamatsu) with the sensitivity peaking at 420 nm [magenta curve in Fig. 3(a)]. The control voltage is set between 0.5–0.7 V for linearly approximate small gain to avoid signal saturation. Signal photons are collected by PMTs and converted to electric signal, which is further amplified by transimpedance amplifier with 30200 V/A (TIA60, Thorlabs). A data acquisition card (PCIe-6321, National Instruments) acts as an analog-to-digital converter with 14-bit resolution (i.e., intensity of each image pixel varies from 0 to 16383).

III. Experimental Results

We first demonstrate that the fiber-based SESS source tuned to 1.25 μm is able to drive HGM imaging in human skin. Then we compare the imaging excited by different wavelength in the range of 1.15–1.35 μm.

A. HGM in Human Skin Excited by 1.25-μm Fiber-Based SESS Source

Figure 4 shows four representative HGM images of *ex vivo* human skin tissue from the back part. Each image has a field of view (FOV) of 270 μm × 270 μm. The excitation is tuned to

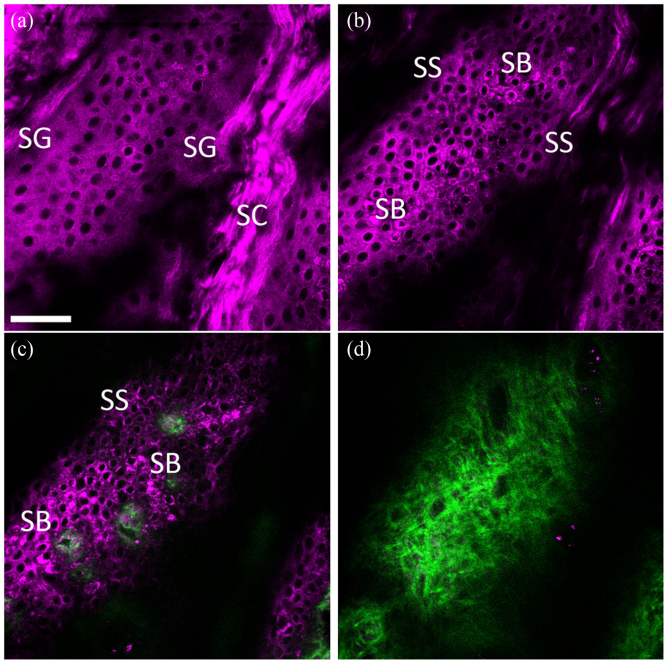

Fig. 4. HGM imaging of *ex vivo* human skin from the back part at different penetration depth excited by 1.25-μm femtosecond pulses. (a) SC and SG in epidermis at 20-μm depth. (b) SS and SB in epidermis at 39-μm depth. (c) SS, SB, and DP between epidermis and dermis at 62-μm depth. (d) Collagen fibers in dermis at 113-μm depth. Scale bar: 50 μm.

1.25 μm—the typical center wavelength of Cr:forsterite lasers. The excitation power is 50 mW, corresponding to 1.6-nJ pulse energy after the objective. The resulting SHG at 625 nm is colored in green, and the THG at 417 nm colored in magenta. We use the same topping color of SHG and THG for the following HGM imaging in this paper.

The THG signal exhibits a strong contrast from the cell in epidermis [Fig. 4(a), 4(b), and 4(c)]. Different sublayers and cells in epidermis can be differentiated by the THG contrast. For example, SC can be easily recognized by its nucleiless feature, and granular cells have a relatively lower nucleus-cytoplasmic ratio compared with spinous cells and basal cells. At 20-μm depth, SC and SG can be simultaneously observed shown in Fig. 4(a). At 39-μm depth, the major cells are spinous and basal cells [Fig. 4(b)]. SHG originating from the collagen fibers starts to appear as the depth increases to 62 μm. These fibers are surrounded by basal cells, showing the uneven region of dermal papillae (DP) at the edge between epidermis and dermis [Fig. 4(c)]. For the imaging depth increased to 113 μm, THG signal vanishes and is replaced by SHG from abundant collagen fibers [Fig. 4(d)].

Figure 5 shows the HGM imaging (FOV: 270 μm $\times$ 270 μm) similar to Fig. 4, but the skin sample is from the inguinal part. The excitation power is also 50 mW. Both the red blood cell and lipids can be observed in the capillary surrounded by the collagen fiber [Fig. 5(c) and 5(d)]. They can be easily distinguished by the size. THG signals are also related to the endogenous molecules (e.g., melanin [4], [6], hemoglobin [39], and lipid [40]), and can be resonantly enhanced by excitation in the 1.15–1.35 μm wavelength range. To emphasize the

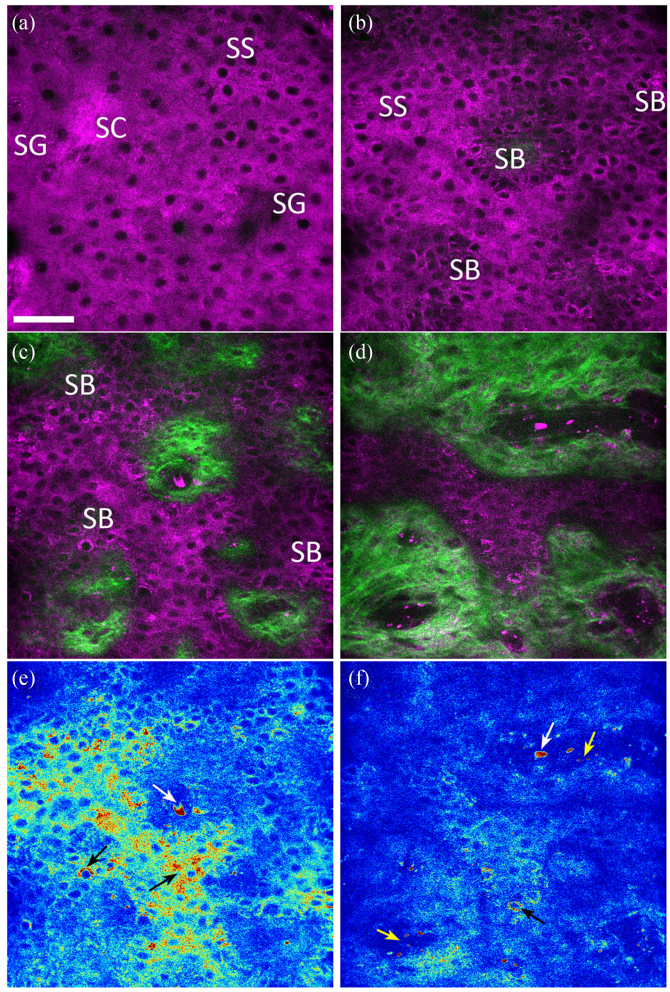

Fig. 5. HGM imaging of *ex vivo* human skin from the inguinal part at different penetration depth excited by 1.25-μm femtosecond pulses. (a) SC, SG and SS in epidermis at 25-μm depth. (b) SS and SB in epidermis at 46-μm depth. (c) DP consists of SB and collagen fibers between epidermis and dermis at 58-μm depth. (d) Capillaries surrounded by collagen fibers at 98-μm depth. (e) and (f) are at the same depth with (c) and (d), respectively. Only THG contrast is reserved and "Jet" colormap is used to emphasize the molecule-induced resonance enhancement. Scale bar: 50 μm.

molecule-induced resonance enhancement, we reserve only the THG contrast in Fig. 5(e) and 5(f), and change the colormap from magenta to "Jet." Consequently, the melanin-induced resonant enhancement in SB can be used to distinguish melanocytes from keratinocytes by the THG contrast. Strong THG colored in red indicates the melanocytes and melanin distribution among the surrounding keratinocytes indicated by black arrows in Fig. 5(e) and 5(f), as well as red blood cells (white arrows) and lipids (yellow arrows).

The HGM imaging excited by 1.25-μm fiber-based SESS source shows similar penetrability and subcellular resolution to differentiate cells and tissues in human skin, comparable to those achieved from Cr:forsterite lasers [4], [6].

B. *Effect of Excitation Wavelength*

To compare the performance of different excitation wavelengths, we observe the sample irradiated by 5 different

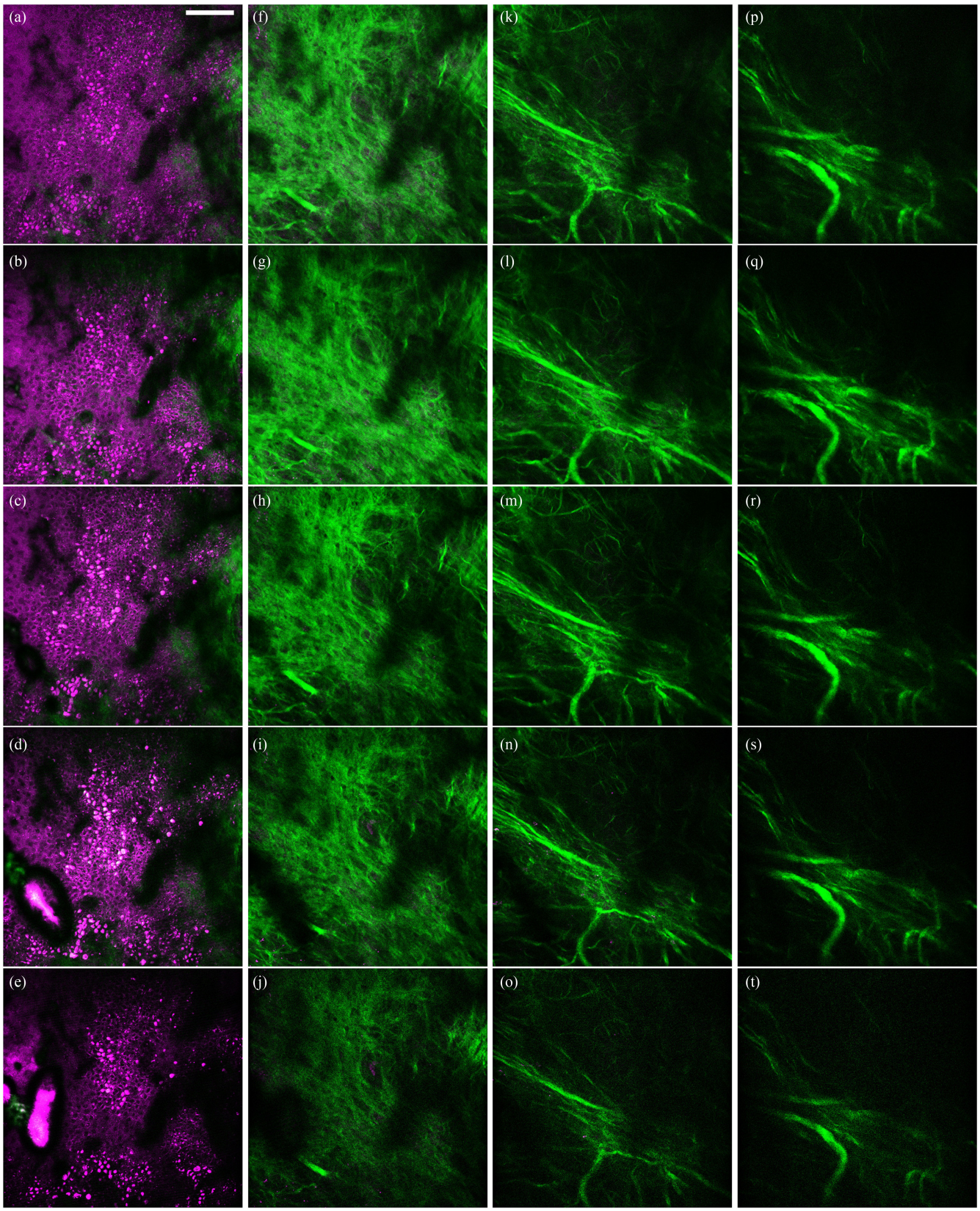

Fig. 6. HGM imaging of *ex vivo* human skin from the back part at different penetration depth excited by 5 different wavelengths. (a-e) SS and SB in epidermis at 50-μm depth. (f-j) Collagen fibers in dermis at 90-μm depth. (k-o) Collagen fibers and arrector pili muscles in dermis at 120-μm depth. (p-t) Arrector pili muscles in dermis at 170-μm depth. 1.15-μm excitation: (a), (f), (k), and (p). 1.2-μm excitation: (b), (g), (l), and (q). 1.25-μm excitation: (c), (h), (m), and (r). 1.3-μm excitation: (d), (i), (n), and (s). 1.35-μm excitation: (e), (j), (o), and (t). Scale bar: 100 μm.

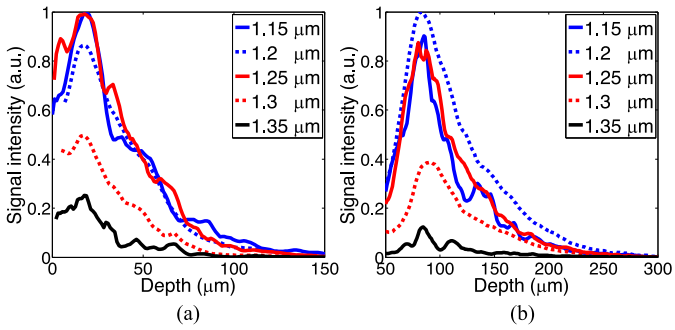

Fig. 7. Signal intensity distribution along the penetration depth depending on different excitation. (a) THG. (b) SHG.

wavelengths peaking at 1.15 μm, 1.2 μm, 1.25 μm, 1.3 μm, and 1.35 μm. The region of interest is scanned back and forth within the penetration depth up to 300 μm. Considering both the microscope transmittance and the pulse duration, we use a neutral density wheel to adjust the illumination power at these wavelengths to maintain the same pulse peak power after the objective. The excitation power of 1.15-μm, 1.2-μm, 1.25-μm, and 1.3-μm pulses is 60 mW after the objective. For 1.35-μm pulses, the applied power is 70 mW.

Figure 6 shows the HGM imaging (FOV: 500 μm $\times$ 500 μm) of *ex vivo* human skin from the back part excited by different wavelengths at four representative penetration depths. Figure 6(a-e) shows the SS and SB at 50-μm depth in epidermis, Fig. 6(f-j) the collagen fibers at 90-μm depth, Fig. 6(k-o) the collagen fibers and arrector pili muscles at 120-μm depth, and Fig. 6(p-t) the arrector pili muscles at 170-μm depth.

At first glance, the resulting HGM images excited by different wavelengths seem similar. However, image details reveal significant difference. Besides the strong THG contrast from various cells in Fig. 6(a-e) as predicted, air bubbles appear at the lower left corner of Fig. 6(d) and 6(e) for 1.3-μm and 1.35-μm excitation, indicating strong water absorption as the excitation wavelength becomes close to a local peak absorption at 1.45 μm [41]. We attribute the generation of air bubbles to water vaporization at the local volume. Since the refractive index difference between air and water or air and skin is larger [42], the air-water or air-skin interface can result in strong THG, and thus suppresses the THG contrast of the cells. These air bubbles also degrade the NA of the water immersive objective in the local area, resulting in weak SHG in deeper layers [Fig. 6(i) and 6(j)], compared with [Fig. 6(f-h)]. Although the outline of the thick arrector pili muscles is still clear in Fig. 6(n) and 6(o), the contrast is worsened especially compared with Fig. 6(k-m). In addition, the fine structure of collagen fibers excited by 1.35-μm femtosecond pulses [Fig. 6(j)] is apparently vaguer than others achieved by pulses of shorter excitation wavelength.

To quantify the effect of excitation wavelength, we plot the signal intensity distribution along the penetration depth in Fig. 7. The signal intensity is defined as pixel intensity summation of the image at each depth. Although the intensity peak of THG [Fig. 7(a)]/SHG [Fig. 7(b)] excited by different wavelength is all at 20-μm/90-μm depth, their relative intensities are substantially different. The signal intensity is much lower for those excited by 1.3-μm and 1.35-μm femtosecond pulses caused by the increased water absorption. Besides the conventional 1.25-μm excitation (which is traditionally offered by Cr:forsterite lasers), 1.15-μm and 1.2-μm excitations enable similar imaging quality given the same peak power after the objective.

IV. Conclusion

We demonstrate a wavelength widely tunable femtosecond source employing SESS for HGM imaging in human skin. The resulting spectrum can be continuously tuned between 1.15 μm and 1.35 μm—covering one of the biological transmission windows—with up to >10-nJ pulse energy and ~100-fs pulse duration. The HGM imaging differentiates various cells and tissues in epidermis and upper dermis of human skin. We compare HGM imaging of *ex vivo* human skin tissue by different excitation in the range of 1.15–1.35 μm with the same peak after the objective. Besides 1.25 μm, our result suggests a ~100-nm wide sub-window between 1.15 μm and 1.25 μm suitable for conducting HGM in human skin. Indeed, femtosecond pulses within 1.15–1.25 μm can also be generated by an Yb-fiber laser based SESS source [35]. However, optical fibers usually exhibit higher positive GVD at this pump wavelength (i.e., 1.03 μm), which leads to stretched pulses and reduced spectral broadening. Additionally, the self-focusing threshold is ~4 MW at the Yb-fiber laser wavelength and ~9 MW at the Er-fiber laser wavelength [43]. Therefore SESS based on Er-fiber lasers exhibits better energy scalability. Femtosecond pulses with MW-peak power at 1.3 μm are demonstrated in our previous work by implementing SESS in 1.3-cm DSF [37]. Considering self-focusing and 15% conversion efficiency, the allowed peak power of 1.3-μm pulses enabled by current approach is ~1.3 MW.

A local minimum of water absorption around 1.1 μm is also attractive to HGM. However, shorter wavelength signifies higher photon energy and increase the risk of photodamage. For long-term observation, power tolerance study (e.g., experimental investigation in [8], [9]) is inevitable. Another issue is whether the resulting THG signal in UV region is harmful to the cell. UVA (320–400 nm) accounts for 95% of the UV radiation reaching the Earth surface. It has higher penetrability than UVB (290–320 nm). Although UVA does not directly harm the skin surface, it may damage keratinocytes and contribute to the initiation of skin cancer development [44].

In our current implementation, femtosecond pulses in 1.15–1.35 μm are obtained by optically filtering the leftmost spectral lobes of an SPM broadened spectrum. If the rightmost spectral lobes are selected using suitable optical bandpass filters, we can obtain femtosecond pulses tunable in 1.6–1.7 μm, which falls into another tissue transmission window of 1.6–1.87 μm [10]–[12]. However, excitation for HGM in this wavelength range exhibits stronger water absorption, and gallium arsenide PMT has lower sensitivity for the corresponding SHG (800-935 nm) signal [45].

Currently we are upgrading our Er-fiber laser system to 1-μJ level with variable repetition rate to implement a SESS source with all the important laser parameters—center wavelength, pulse duration, pulse energy, and average power—flexibly ad-

justable. Such a powerful driving source allows us further optimizing the HGM performance in human skin imaging, which will constitute a powerful tool to conduct noninvasive optical virtual biopsy to study histopathology, morphology, and skin disease.

ACKNOWLEDGMENT

The authors thank S. Degenhardt, S. Henning, and I.-P. Chen for preparing the sample.

REFERENCES

[1] E. Brown *et al.*, "Dynamic imaging of collagen and its modulation in tumors *in vivo* using second-harmonic generation," *Nature Med.*, vol. 9, no. 6, pp. 796–800, 2003.

[2] C.-K. Sun *et al.*, "Multiharmonic-generation biopsy of skin," *Opt. Lett.*, vol. 28, no. 24, pp. 2488–2490, 2003.

[3] S.-P. Tai *et al.*, "Optical biopsy of fixed human skin with backward-collected optical harmonics signals," *Opt. Express*, vol. 13, no. 20, pp. 8231–8242, 2005.

[4] S.-Y. Chen, H.-Y. Wu, and C.-K. Sun, "*In vivo* harmonic generation biopsy of human skin," *J. Biomed. Opt.*, vol. 14, no. 6, pp. 060505-1–060505-3, 2009.

[5] T. Yasui, Y. Takahashi, M. Ito, S. Fukushima, and T. Araki, "*Ex vivo* and *in vivo* second-harmonic-generation imaging of dermal collagen fiber in skin: Comparison of imaging characteristics between mode-locked Cr:forsterite and Ti:sapphire lasers," *Appl. Opt.*, vol. 48, no. 10, pp. D88–D95, 2009.

[6] S.-Y. Chen *et al.*, "*In vivo* virtual biopsy of human skin by using noninvasive higher harmonic generation microscopy," *IEEE J. Sel. Topics Quantum Electron.*, vol. 16, no. 3, pp. 478–492, May/Jun. 2010.

[7] M.-R. Tsai, S.-Y. Chen, D.-B. Shieh, P.-J. Lou, and C.-K. Sun, "*In vivo* virtual biopsy of human oral mucosa with harmonic generation microscopy," *Biomed. Opt. Express*, vol. 2, no. 8, pp. 2317–2328, 2011.

[8] C.-S. Hsieh, S.-U. Chen, Y.-W. Lee, Y.-S. Yang, and C.-K. Sun, "Higher harmonic generation microscopy of *in vitro* cultured mammal oocytes and embryos," *Opt. Express*, vol. 16, no. 15, pp. 11574–11588, 2008.

[9] K. König, P. T. C. So, W. W. Mantulin, and E. Gratoon, "Cellular response to near-infrared femtosecond laser pulses in two-photon microscopes," *Opt. Lett.*, vol. 22, no. 2, pp. 135–136, 1997.

[10] R. R. Anderson and J. A. Parrish, "The optics of human skin," *J. Investigative Dermatology*, vol. 77, no. 1, pp. 13–19, 1981.

[11] L. A. Sordillo, Y. Pu, S. Pratavieira, Y. Budansky, and R. R. Alfano, "Deep optical imaging of tissue using the second and third near-infrared spectral windows," *J. Biomed. Opt.*, vol. 19, no. 5, pp. 056004-1–056004-6, 2014.

[12] L. Shi, L. A. Sordillo, A. Rodríguez-Contreras, and R. Alfano, "Transmission in near-infrared optical windows for deep brain imaging," *J. Biophotonics*, vol. 9, no. 1/2, pp. 38–43, 2016.

[13] N. G. Horton *et al.*, "*In vivo* three-photon microscopy of subcortical structures within an intact mouse brain," *Nature Photon.*, vol. 7, no. 3, pp. 205–209, 2013.

[14] K. Wang, N. G. Horton, K. Charan, and C. Xu, "Advanced fiber soliton sources for nonlinear deep tissue imaging in biophotonics," *IEEE J. Sel. Topics Quantum Electron.*, vol. 20, no. 2, Mar./Apr. 2014, Art. no. 6800311.

[15] D. G. Ouzounov *et al.*, "*In vivo* three-photon imaging of activity of GCaMP6-labeled neurons deep in intact mouse brain," *Nature Methods*, vol. 14, no. 4, pp. 388–390, 2017.

[16] S.-W. Chu *et al.*, "Multimodal nonlinear spectral microscopy based on a femtosecond Cr:forsterite laser," *Opt. Lett.*, vol. 26, no. 23, pp. 1909–1911, 2001.

[17] S.-W. Chu *et al.*, "Nonlinear bio-photonic crystal effects revealed with multi-modal nonlinear microscopy," *J. Microsc.*, vol. 208, pp. 190–200, 2002.

[18] C.-K. Sun *et al.*, "Higher harmonic generation microscopy for developmental biology," *J. Struct. Biol.*, vol. 147, pp. 19–30, 2004.

[19] D. Yelin and Y. Silberberg, "Laser scanning third-harmonic-generation microscopy in biology," *Opt. Express*, vol. 5, no. 8, pp. 169–175, 1999.

[20] L. Canioni *et al.*, "Imaging of Ca^{2+} intracellular dynamics with a third-harmonic generation microscope," *Opt. Lett.*, vol. 26, no. 8, pp. 515–517, 2001.

[21] H. T. Chen *et al.*, "A multimodal platform for nonlinear optical microscopy and microspectroscopy," *Opt. Express*, vol. 17, no. 3, pp. 1282–1290, 2009.

[22] D. Kobat *et al.*, "Deep tissue multiphoton microscopy using longer wavelength excitation," *Opt. Express*, vol. 17, no. 16, pp. 13354–13364, 2009.

[23] M. Müller, J. Squier, K. R. Wilson, and G. J. Brakenhoff, "3D-Microscopy of transparent objects using third-harmonic generation," *J. Microsc.*, vol. 191, no. 3, pp. 266–274, 1998.

[24] J. A. Squier, M. Müller, G. J. Brakenhoff, and K. R. Wilson, "Third harmonic generation microscopy," *Opt. Express*, vol. 3, no. 9, pp. 315–324, 1999.

[25] H.-Y. Wang, S-.W. Huang, D.-R. Li, B.-S. Lin, and M.-C. Chan, "Nonlinear light microscopy by a 1.2-μm fiber-laser-based femtosecond dispersive wave source," *IEEE Photon. J.*, vol. 7, no. 3, Jun. 2015, Art. no. 6900608.

[26] T.-M. Tsai, D.-R. Li, and M.-C. Chan, "Non-invasive image-guided laser microsurgery by a dual-wavelength fiber laser and an integrated fiber-optic multi-modal system," *Opt. Lett.*, vol. 41, no. 20, pp. 4847–4850, 2016.

[27] H. Lim, F. O. Ilday, J. Buckley, A. Chong, and F. W. Wise, "Fiber-based source of femtosecond pulses tunable from 1.0 to 1.3 μm," *Electron. Lett.*, vol. 40, no. 24, pp. 1523–1525, 2004.

[28] J. Takayanagi, T. Sugiura, M. Yoshida, and N. Nishizawa, "1.0–1.7-μm wavelength-tunable ultrashort-pulse generation using femtosecond Yb-doped fiber laser and photonic crystal fiber," *IEEE Photon. Technol. Lett.*, vol. 18, no. 21, pp. 2284–2286, Nov. 2006.

[29] K.-C. Li, L. L. H. Huang, J.-H. Liang, and M.-C. Chang, "Simple approach to three-color two-photon microscopy by a fiber-optic wavelength convertor," *Biomed. Opt. Express*, vol. 7, no. 11, pp. 4803–4815, 2016.

[30] M. E. V. Pedersen *et al.*, "Higher-order-mode fiber optimized for energetic soliton propagation," *Opt. Lett.*, vol. 37, no. 16, pp. 3459–3461, 2012.

[31] L. Rishøj, B. Tai, P. Kristensen, and S. Ramachandran, "Characterization of intermodal group index matched soliton interactions leading to MW peak powers at 1300 nm," in *Proc. Conf. Lasers Electro-Opt.*, 2017, Paper STh3K.2.

[32] J.-Y. Huang *et al.*, "Fiber-based 1150-nm femtosecond laser source for the minimally invasive harmonic generation microscopy," *J. Biomed. Opt.*, vol. 22, no. 3, pp. 036008-1–036008-8, 2017.

[33] P. Mamyshev, "All optical data regeneration based on self-phase modulation effect," in *Proc. Eur. Conf. Opt. Commun.*, Madrid, Spain, 1998, pp. 475–476.

[34] W. Liu, C. Li, Z. Zhang, F. X. Kärtner, and G. Q. Chang, "Self-phase modulation enabled, wavelength-tunable ultrafast fiber laser sources: An energy scalable approach," *Opt. Express*, vol. 24, no. 14, pp. 15328–15340, 2016.

[35] W. Liu *et al.*, "Energetic ultrafast fiber laser sources tunable in 1030–1215 nm for deep tissue multi-photon microscopy," *Opt. Express*, vol. 25, no. 6, pp. 6822–6831, 2017.

[36] H.-Y. Chung, W. Liu, Q. Cao, F. X. Kärtner, and G. Q. Chang, "Er-fiber laser enabled, energy scalable femtosecond source tunable from 1.3 to 1.7 μm," *Opt. Express*, vol. 25, no. 14, pp. 15760–15771, 2017.

[37] H.-Y. Chung *et al.*, "Megawatt peak power tunable femtosecond source based on self-phase modulation enabled spectral selection," *Opt. Express*, vol. 26, no. 3, pp. 3684–3695, 2018.

[38] 2018. [Online]. Available: http://www.hamamatsu.com/us/en/index.html

[39] R. D. Schaller, J. C. Johnson, and R. J. Saykally, "Nonlinear chemical imaging microscopy: Near-field third harmonic generation imaging of human red blood cells," *Anal. Chem.*, vol. 72, no. 21, pp. 5361–5364, 2000.

[40] D. Débarre *et al.*, "Imaging lipids bodies in cells and tissues using third-harmonic generation microscopy," *Nature Methods*, vol. 3, no. 1, pp. 47–53, 2006.

[41] L. Kou, D. Labrie, and P. Chylek, "Refractive indices of water and ice in the 0.65- to 2.5-μm spectral range," *Appl. Opt.*, vol. 32, no. 19, pp. 3531–3540, 1993.

[42] H. Ding, J. Q. Lu, W. A. Wooden, P. J. Kragel, and X.-H. Hu, "Refractive indices of human skin tissues at eight wavelengths and estimated dispersion relations between 300 and 1600 nm," *Phys. Med. Biol.*, vol. 51, no. 6, pp. 1479–1489, 2006.

[43] A. V. Smith, B. Do, G. Hadley, and R. L. Farrow, "Optical damage limits to pulse energy from fibers," *IEEE J. Sel. Topics Quantum Electron.*, vol. 15, no. 1, pp. 153–158, Jan. 2009.

[44] 2013. [Online]. Available: https://www.skincancer.org/prevention/uva-and-uvb

[45] Y. Wang, K. Wang, W. Wen, P. Qiu, and K. Wang, "Comparison of signal detection of GaAsP and GaAs PMTs for multiphoton microscopy at 1700-nm window," *IEEE Photon. J.*, vol. 8, no. 3, Jun. 2016, Art. no. 6803406.

Hsiang-Yu Chung received the B.S. degree in physics and the M.S. degree in photonics and optoelectronics from National Taiwan University, Taipei, Taiwan, in 2010 and 2013, respectively. Since 2014, he has been working toward the Ph.D. degree in physics with Universität Hamburg, Hamburg, Germany. His research interests include high-power ultrafast fiber lasers, nonlinear fiber optics, and development of fiber-based light source for nonlinear optical microscopy.

Wei Liu was born in Hubei, China, in 1985. He received the B.S. degree in physics from Sun Yan-Sen University, Guangzhou, China, in 2009, the M.S. degree in optical engineering from Zhejiang University, Hangzhou, China, in 2012, and the Ph.D. degree in physics from DESY/Hamburg University, Hamburg, Germany, in 2016. Since 2017, he has been a Research Associate with SLAC National Laboratory, Stanford University, Stanford, CA, USA, where he currently works on coherent ultrafast pulse combining, frequency comb, and ultrafast fiber laser for accelerator related application.

Qian Cao received the B.Sc. degree from the Department of Optical Science and Engineering, Fudan University, Shanghai, China, in 2012, and the M.Sc. degree in electro-optics program, University of Dayton, Dayton, OH, USA, in 2014. Since 2014, he has been currently working toward the Ph.D. degree in physics with Universität Hamburg, Hamburg, Germany. He is currently a Research Assistant with Prof. Franz Kaertner's Ultrafast Optics and X-rays (UFOX) Group. He is also a student with the International Max Planck Research School and PIER Helmholtz Graduate School. His research interests include fiber lasers, laser noise, optical parametric process, spatiotemporal wave packets, and ultrafast optics. He was the recipient of the graduate student fellowship from PIER Helmholtz Graduate School in 2015.

Rüdiger Greinert received the Diploma and Ph.D. degrees in physics from the University of Göttingen, Göttingen, Germany, in 1979 and 1982, respectively. He currently heads the Department of Molecular Cellbiology, Skin Cancer Center, Elbekliniken Stade/Buxtehude, Buxtehude, Germany, and also the Member of the Board of Directors of the German Association of Dermatological Prevention (ADP e.V.) and the Secretary General of the European Society of Skin Cancer Prevention. His research interest includes the study of molecular mechanisms of UV-induced skin cancer, especially the involvement of epigenetic regulation of human epidermal and dermal stem cell fate.

Franz X. Kärtner (F'09) heads the Ultrafast Optics and X-Rays Group, Center for Free-Electron Laser Science, DESY, Hamburg, Germany, and is currently a Professor with the Physics Department, Universität Hamburg, Hamburg, Germany, and an Adjunct Professor in electrical engineering with the Massachusetts Institute of Technology, Cambridge, MA, USA. His research interests include noise in electronic and optical sources, ultrashort pulse lasers, high-energy subcycle waveform synthesis, frequency combs and precision timing in advanced accelerators and light sources, attosecond physics, and compact free-electron lasers.

Guoqing Chang received both the Bachelor's and the Master's degrees from the Department of Electronics Engineering, Tsinghua University, Beijing, China, and the Ph.D. degree in electrical engineering from the Center for Ultrafast Optical Science, University of Michigan, Ann Arbor, MI, USA. He is currently a Professor with the Institute of Physics (IOP), Chinese Academy of Sciences, Beijing, China. After staying at the University of Michigan as a Postdoctoral Research Fellow for about one year, he joined the Research Laboratory of Electronics, MIT, as a Postdoctoral Research Associate. In August 2012, he moved to the Center for free electron laser at Hamburg (Germany) as the Head of the Helmholtz Young investigator group "Ultrafast Laser Optics and Coherent Microscopy." He was granted tenure in December 2016. Recently, he joined IOP through "Hundred Talents Program."